Title

RETAINED AUSTENITE AND TEMPERED MARTENSITE EMBRITTLEMENT IN MEDIUM CARBON STEELS

Authors

Sarikaya, M.
Jhingan, A.K.
Thomas, G.

Publication Date

1982-11-01

Lawrence Berkeley Laboratory
UNIVERSITY OF CALIFORNIA

Materials & Molecular Research Division

Submitted to Metallurgical Transactions

RETAINED AUSTENITE AND TEMPERED MARTENSITE EMBRITTLEMENT IN MEDIUM CARBON STEELS

M. Sarikaya, A.K. Jhingan, and G. Thomas

November 1982

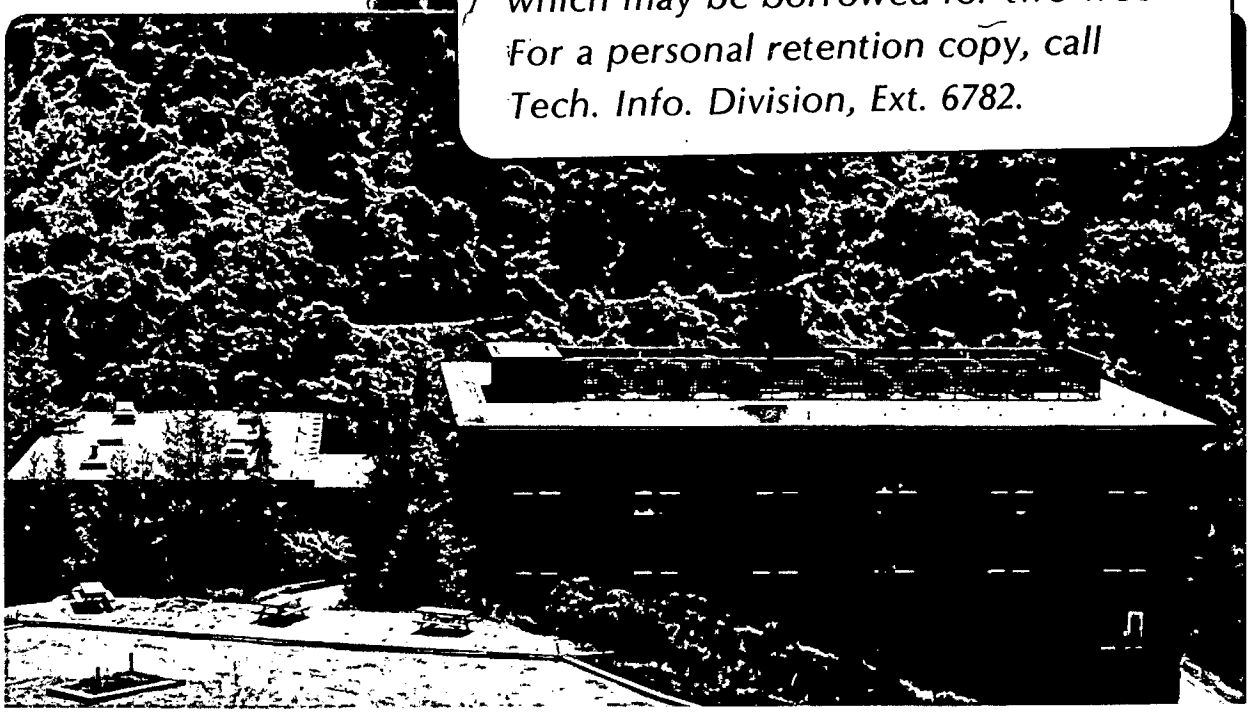

Prepared for the U.S. Department of Energy under Contract DE-AC03-76SF00098

DISCLAIMER

LBL-13876

RETAINED AUSTENITE AND TEMPERED MARTENSITE EMBRITTLEMENT IN MEDIUM CARBON STEELS

M. Sarikaya, A.K. Jhingan, and G. Thomas

Lawrence Berkeley Laboratory
University of California
Berkeley, California 94720

November 1982

This work was supported by the U.S. Department of Energy under Contract No. DE-AC03-76SF00098.

RETAINED AUSTENITE AND TEMPERED MARTENSITE EMBRITTLEMENT IN MEDIUM CARBON STEELS.

M. SARIKAYA, A.K. JHINGAN, AND G. THOMAS

ABSTRACT: Electron microscopy, diffraction and microanalysis, X-ray diffraction, and auger spectroscopy have been used to study quenched and quenched and tempered 0.3% carbon low alloy steels. Some in-situ fracture studies were also carried out in a high voltage electron microscope.

Tempered martensite embrittlement (TME) is shown to arise primarily as a microstructural constraint associated with decomposition of interlath retained austenite into M_3C films upon tempering in the range of 250°C-400°C. In addition, intralath Widmanstatten Fe_3C forms from epsilon carbide. The fracture is transgranular with respect to prior austenite. The situation is analogous to that in upper bainite. This TME failure is different from temper embrittlement (TE) which occurs at higher tempering temperatures (approximately 500°C), and is not a microstructural effect but rather due to impurity segregation (principally sul - phur in the present work) to prior austenite grain boundaries leading to intergranular fracture along those boundaries. Both failures can occur in the same steels, depending on the tempering conditions .

INTRODUCTION

It has already been shown that TME in experimental 0.3% C and commercial structural steels (such as AISI 4340)[1-3] is associated with decomposition

M. Sarikaya and A.K. Jhingan are graduate students, and G. Thomas is Professor of Metallurgy, Department of Materials Science & Mineral Engineering, University of California, Berkeley, CA 94720.

of retained austenite into carbides. However, the correlation of microstructural and morphological changes with mechanical properties, especially fracture, still requires some elucidation. It is the objective of the present work to examine these details using characterization techniques including electron microscopy, diffraction, microanalysis, X-rays, and Auger spectroscopy. The steels chosen are based on alloys designed to combine attractive combinations of strength and toughness.[4] They are primarily low alloy steels of approximately 0.3% C, so as to provide dislocated lath martensite and interlath retained austenite upon quenching from the austenite range. The basis for the design of these steels is described elsewhere.[4,5]

The mechanical properties, especially fracture, of these steels depend strongly upon composition and temperature for tempering above approximately 250°C. Sudden troughs in the toughness (measured as Charpy V-notch impact energy or plane strain fracture toughness[6]) vs. tempering temperature curves are observed either in the vicinity of 350°C tempering[1-5,7-17] or 500°C tempering, or both, depending on the alloying additions (e.g., Cr, Mn, Mo, Ni, Si, etc.), extent of impurity content (e.g., S, P, Sb, Sn, As) and the history of the heat treatments, especially austenitizing temperature. This embrittlement[1,8,18] subsequently causes an increase in the ductile-to-brittle transition temperature (DBTT) of the steels.

The embrittlement which occurs with tempering in the vicinity of 500°C is called "500°C embrittlement" or more generally "temper embrittlement" (TE) which is usually attributed to the segregation of impurity elements to the prior austenite grain boundaries causing predominantly intergranular fracture (with respect to preaustenite grain boundaries[8,9,11,12,18]).

This embrittlement commonly occurs in low purity commercial steels, and the extent and the temperature of the embrittlement depends on the impurity level in the bulk alloys. The embrittlement on tempering near 350°C is termed "tempered martensite embrittlement" (TME).[1-3,8,9,11,14,23] Since this embrittlement can be found in high purity vacuum-melted alloys[1,2] it is not considered to be controlled by impurities. In the case of TME the fracture path is quasi-cleavage, transgranular with respect to the prior austenite grains, and having a morphology characteristic of the underlying packet lath martensite structure. There are some controversies regarding the details of the mechanism of TME, namely whether it is impurity controlled[11-13,17], whether it depends on the tempered intralath carbides (e.g., epsilon-cementite transition) and rapid coarsening, or is due to decomposition of the interlath retained austenite films leading to microstructures similar to brittle upper bainite.[1] These interlath carbides may either provide crack nucleation sites[1,14,16,22] and/or easy crack paths.[1,3,4,15]

The beneficial effects of retained austenite films, which remain after quenching at the martensite lath boundaries, on the toughness values[1,4,5,22] can thus be lost due to its decomposition on tempering, concurrent with TME in these steels.[1-5,24-27] It is the purpose of this paper to present more quantitative results on the effect of retained austenite decomposition on the TME and to distinguish this embrittlement from TE.

EXPERIMENTAL PROCEDURE

The experimental alloys were vacuum induction melted in 9.0 kg ingots and subsequently rolled to 2.5 cm thick, 6.25 cm wide, and 62.5 cm

long slabs, which were then homogenized at 1200°C for 24 hours in vacuum before furnace cooling. The compositions given in Table 1 were measured after homogenization. The C content of the alloys was measured after each austenitization process. The transformation temperatures, i.e., Ms, Mf, As, and Af (Table 1) were measured by standard dilatometry.

Specimens for the mechanical tests were cut from the homogenized material and machined to blanks which were then austenitized at 1100°C for 1 hour in a vertical tube furnace under a dynamic argon atmosphere. Quenching was done in agitated oil. The resulting austenite grain sizes were 270, 180, and 300 μm for alloys V1, V2, and V3, respectively. Isothermal and isochronal tempering treatments were done in a salt pot and then the specimens were quickly quenched into water. Final machining was done under flood cooling to avoid any heating.

Standard ASTM size specimens were used to measure the Charpy V-notch impact energies[6] (the long axis of the test specimens was parallel to the rolling direction, and the base of the notch was perpendicular to the surface). Testing was conducted with a 224 ft-lb capacity impact machine at room temperature. Broken impact specimens were then examined for fractography in an AMR-1000 scanning electron microscope operated at 20 kV.

Microstructural examinations were conducted by optical and transmission electron microscopy (TEM) techniques. Thin foils for TEM were obtained from the broken impact specimens. Slices of ~ 0.020 inch (500 μm) were cut longitudinally with a 1/32 inch (800 μm) thick abrasive wheel under flood cooling. 3 mm discs were then "spark cut" from

Table 1. Composition and Transformation Temperatures of the Three Steels Used in This Study

	C	Cr	Mn	Ni	Mo	Si	Cu	Al	P	S	N	Fe	Transformation Temperatures, °C Ms	Mf	As	Af
V1*	0.26	3.11	1.98	0.01	0.50	0.07	0.01	----	0.007	0.011	----	bal	320	260	765	800
V2*	0.25	3.01	0.08	2.00	0.51	0.07	0.01	----	0.007	0.009	----	bal	340	260	780	820
V3**	0.29	2.97	2.10	----	----	0.01	----	0.027	0.003	0.007	0.001	bal	330	206	732	790

*Supplied by Daido Steel Company, Japan

**Supplied by Japan Steel Works, Japan

these slices which were already chemically thinned to about 0.1 mm in 5% HF-H_2O_2 solution. Discs were then carefully sanded down to about 0.05 mm and then electropolished in a twin jet electropolishing apparatus at room temperature in a chromic-acetic solution (75 gm CrO_3 + 400 ml CH_3-COOH + 20 ml H_2O) at a voltage range of 40-45 volts and currents at 50-55 milliamps. Carbide extraction replicas were prepared in the usual way from metallographically polished and overetched (in 5% nital) specimens. Transmission electron microscopy, diffraction, and microanalysis[28,29] were done on the Philips EM 301 and 400 microscopes operated at 100 kV. Foils made from bulk heat-treated samples were deformed to fracture in-situ in a high voltage electron microscope* so that some idea might be obtained of the fracture mechanisms. Some results of this latter work were also reported recently at the Liverpool Conference.[30] Quantitative X-ray microanalysis interpretation requires careful analysis for corrections due to fluorescence, foil thickness, etc.[28,29] In the present case the correction factors for Cr and Mn were found to be 1.43 and 1.30, respectively.

Quantitative analysis of the amount of retained austenite was done by X-ray diffraction[31] using a Picker X-ray diffractometer with Cu K_α radiation. This radiation allows better resolution to be made between martensite and austenite reflections. In the present work the reflections used for analysis were {112}, {220}, and {200} martensite, and {220}, {311}, and {200} austenite.

---

*A movie film has been made and is available from the authors.

Auger electron spectroscopy (e.g., Refs. 11,12) was used to analyze the fractured surfaces of the specimens exposed to different embrittlement conditions. Auger spectra were obtained using a primary beam of 5 kV and 400 nanoamps, and a modulation signal of 15 KHZ and 6 volts, peak to peak.

Field ion microscopy using atom probe analysis, especially to determine carbon distributions, was performed as described in Reference 32.

RESULTS

A. Microstructure

The microstructure of the present steels is typical of that of packet martensites, now very well described in the literature. At the light optical level (Figure 1) as-quenched steels consist of packets of martensite within the prior austenite. At the electron optical level, these packets consist of parallel dislocated laths, thin films of interlath retained austenite and autotempered intralath carbide - mostly epsilon. A typical example of the retained austenite is given in Figure 2 and finer details down almost to atomic resolution, have been made by field ion atom probe, the results which have been published recently[32,33] and so will not be repeated here.

Tempering at 200°C does not change this microstructure appreciably. Retained austenite still exists (untransformed) at the lath boundaries, but in alloys V1 and V3 the epsilon carbides are completely transformed to Fe_3C (Figure 3) as evidenced by selected area microdiffraction and trace analysis. On the other hand, a mixture of both, ε - and Fe_3C carbides have been observed in the Ni containing alloy[4,5] (i.e., V2). Drastic changes occur in the microstructures when the alloys are tempered at higher temperatures. After tempering 1 hour, at 300°C the retained

austenite no longer exists in the 2% Mn alloys because it decomposes into stringers of interlath carbides. The carbides within the laths grow larger (Figure 4) retaining the {110} Widmanstatten arrangement, whereas in the nickel steel (V2), the austenite decomposition reaction is completed after 1 hour at 400°C. The carbides formed as a result of this decomposition have the Fe_3C structure and possess a common orientation relationship, namely Bagaryatski, with the martensite matrix (Figure 4c). It is clear in this figure that the intralath carbides have grown larger, but also still have the {110} Widmanstatten arrangement as in the Mn alloy. Spheroidization in the alloys starts after 400°C tempering (1 hour), e.g., Figure 5. Higher tempering temperatures causes all carbides, both interlath and intralath, to coarsen and dislocation recovery within the martensite laths becomes resolvable. Energy dispersive X-ray microanalysis was done on the extracted carbides (e.g., Figure 5d) using the STEM mode so that both inter- and intralath carbides could be examined. After all the appropriate corrections were done[28,29], chromium contents of more than 15 wt% and Mn contents in excess of 3 wt% were found in the interlath carbides transformed from the retained austenite in specimens from alloy V3 which were tempered at 400°C for 135 hours. These carbides are thus described as M_3C. This can be expected from the early work on diffusion of Cr, as described in Reference 34. However, no detectable alloying elements other than Fe and C were found in the intralath carbides, so these are concluded to be Fe_3C.

B. Impact Energy Measurements

The results of some of the Charpy tests are plotted in Figure 6. Tempering the steels at 200°C increased the toughness values considerably while there were no appreciable changes in the tensile strengths.[5] The abrupt changes occurring in the impact values are clearly seen. In alloy V1, low impact values are obtained after tempering in the 300-500°C range, while only one minimum was detected in the case of the 2 Ni alloy (V2). The dark field TEM micrographs, inset in Figure 6, were taken from the V1 alloy corresponding to the tempering temperatures shown. While there are still continuous films of retained austenite present after 200°C tempering, large carbides have formed at the lath boundaries after 300°C tempering, due to the decomposition of retained austenite. Spheroidization of carbides (both interlath and intralath) occurs after 400°C tempering. Similar microstructural changes are observed in the 2 Ni-containing alloy except decomposition of the retained austenite starts above 300°C.

In the 2 Mn alloy (V3), Charpy values were also measured in the isothermally treated specimens, tempered at specific temperatures for long times (e.g., $t_T >> 1$ hour). The impact energy values and fracture data are given in Table 2 and Figure 7. High impact energy values are observed after both the 210°C (Table 2) and 240°C 0.5 hour tempering (Figure 7). However, as a result of the prolonged tempering, especially at 240°C, a large drop occurs in impact toughness.

Table 2. Impact Energies of the V3 Steel

After the Heat Treatments shown

T (°C)	t_T (hrs)	Impact Energy ft-lb	Impact Energy Joules	Fracture Surface Appearance (on Fracture Mode)
210	0.5	40.0	54.24	Ductile dimpled rupture.
	26	25.5	34.58	Mainly ductile dimpled rupture, partly quasi-cleavage
240	0.5	42.5	57.63	Ductile-transgranular*
	16	16.0	21.70	Ductile-however, mostly quasi-cleavage
400	0.5	15.5	21.02	Brittle-partly transgranular, partly intergranular*
	85	12.5	16.95	Mostly intergranular*
	135	12.0	16.27	" "
	257	11.0	14.92	Completely intergranular*

*With respect to prior austenite grains

C. Fractography

The above changes in the impact values can be explained by studying the fractured surfaces of the specimens using a scanning electron microscope. Results are summarized in Figure 8. This figure shows the typical ductile (Figure 8a-c), TME (Figure 8d,g,h) and TE (Figure 8f,j) fractures in the steels as a function of heat treatment. Tempering the Mn-containing alloy (V3) at 400°C for 0.5 hour, resulted, not suprisingly, in the same kind of fracture surface appearance as it did when tempered at 300°C, that is mostly quasi-cleavage with many "ridges", which is associated with the TME. Tempering the same alloy at the

same temperature (i.e., 400°C) for very long times (e.g., 135 hours), changed the crack propagation path, that is to intergranular fracture with respect to the preaustenite grain boundaries (Figure 8f). This behavior is always observed in the classical "temper embrittlement" condition. Note, however, that this behavior was never observed in either steel after 1 hour-400°C tempering. Partly intergranular and partly transgranular (with respect to preaustenite grains) fracture surfaces were observed in the 2 Mn steels after 1 hour at 500°C, but after 1 hour at 600°C the fracture became almost all intergranular (i.e., TE - Figure 8i-j). Therefore, TE occurs after tempering the 2 Mn alloys at or above 500°C. The nickel containing alloy (V2) never showed total TE behavior as defined by total intergranular fracture. This is also expected from the shape of the curve in Figure 6.

D. Spectroscopic Analyses

Secondary electron spectroscopy and microscopy were employed on the isothermally aged specimens for chemical analysis of the fractured surfaces. There was no sulphur detected on the fracture surfaces of the specimens which were treated at low temperatures (e.g., 240°C) for longer times (e.g., 26 hours). On the other hand, as Figure 9 shows, sulphur segregation was detected at the flat intergranular facets on the fracture surfaces of the specimens which were tempered at higher temperatures (e.g., 400°C) for longer times (135 hours). The fracture path is intergranular in this condition and is thus due to TE caused by sulphur impurity segregation. Thus, TME in these steels is not associated with this kind of segregation.

It should be noted here that even at 200°C tempering, there is a considerable amount of C partitioning and segregation at the tempered martensite/austenite interface. The C content increases to very high values (approximately 10 wt%) at local regions along the martensite-austenite interfaces. Figure 10 shows an example of a C profile obtained from an actual atom probe analysis across the austenite/martensite interface in 2% Mn steel alloys after 1 hour at 200°C tempering. Here the C level is exceptionally high in austenite (>> nominal 0.3%) and low in the martensite. The local regions containing very high C levels may be the nucleation sites for the eventual carbides which form by decomposition of retained austenite.

The volume fractions of retained austenite were measured by X-ray diffraction after the various tempering conditions and a typical result is given in Figure 11. In the as-quenched (AQ) condition, 3-4 vol% retained austenite was detected in the specimens. However, after tempering the steels at 250°C for different times, the fraction of retained austenite decreased to very low values which could not be quantitatively evaluated with confidence. The results, however, are concurrent with the metallographic observations of the decomposition of retained austenite to interlath carbide and the onset of TME in the steels (Figures 6 and 7).

E. In-Situ Deformation

Experiments have been performed by in-situ deformation to fracture of foils of AQ and tempered steels in a high voltage electron microscope and the fractures compared to bulk behavior. While the details will not be given here (see Ref. 30), the interesting results are that

fracture always occurred within and along the martensite laths following intense localized slip, but the zone size of deformation depends upon microstructure. In the TME condition the fracture is highly localized due to the interlath carbides formed after decomposition of the austenite and which severely restricts slip within a given lath, together with the Widmanstatten intralath carbides which form on the {110} slip planes. Figure 12a schematically shows the main features. Although deformation of thin foils represents plane stress conditions which cannot be directly compared to bulk fracture tests, the results are consistent with the microstructural interpretation developed here. The fractographs (Figure 8d, g-h) corresponding to TME are interpreted as being due to localized deformation and fracture along the lath axes as in Figure 12a, part 2, rather than interphase fracture at lath-interlath M_3C interfaces.

Figure 12a is a schematic summary of the main <u>in-situ</u> fracture studies. When retained austenite is present, slip can easily cross from lath to lath via the austenite because $\{110\}\alpha$ parallels $\{111\}_\gamma$ and {110} are the likely slip planes in martensite. Consequently, the plastic zone can be large and slip is not restricted (Figure 12a, part 1). However, when the austenite decomposes into films of cementite this phase tends to block transfer of slip so that the plastic zone may be confined to a single lath (Figure 12a, part 2). On longer tempering, coarsening of this carbide may again permit transfer of slip from lath to lath (Figure 12a, part 3) and the toughness should increase as observed, e.g., Figure 7.

DISCUSSION

As can be seen from the foregoing section, temper martensite embrittlement occurring at 300-400°C tempering, is associated with the decomposition of retained austenite into carbides at the lath boundaries due to its thermal instability. This instability arises because of the thermodynamical requirements associated with the carbon levels retained after quenching.[35] The main factors affecting fracture appear to be the size and distribution of the carbides (both inter- and intralath) and the effect of this microstructure on slip distribution and crack initiation. This depends on tempering temperature. The coarsening of intralath cementite is detectable in the Mn compared to the Ni-containing steels. These interlath carbides, formed when the retained austenite decomposed, must restrict slip within the laths, i.e., the carbides do not allow easy crossing of slip from lath to lath, unlike the situation before retained austenite decomposes. Hence, the crack initiation is also strongly influenced by the austenite decomposition. It should be noted that as far as this interlath morphology is concerned, the situation is very similar to that of upper bainite which also consists of laths and interlath carbide stringers.

The question of crack initiation is very difficult to resolve in bulk specimens. In-situ studies of fracture in foils[30,36] indicate that fracture occurs at localized, highly necked regions in a martensite lath, but the fracture path, though staying within a lath, does branch and other cracks nucleate in adjacent laths of packets, i.e., crack paths are highly dependent on the microstructure, as is of course the plastic zone. The situation is represented schematically in Figure 12a. Again,

it is emphasized that these results have been obtained in thin foils but the ideas suggested may have some merit in understanding fracture in bulk material. If the thin foil evidence is valid, then the dislocation interaction crack initiation model can be invoked as shown in Figure 12b. As a result of intense localized cross slip within a lath (the localization depends again on the microstructure, notably the distribution of inter- and intralath carbides) and at slip intersections, immobile <110> dislocations can be formed which eventually raise the stress locally to the fracture level. Since the intralath carbides are on {110} traces the fracture is zig-zag along the {110} foil plane.

The in-situ results together with the absence of detectable impurity segregation (the auger data) in TME bulk specimens indicates that decohesion due to an increase in interfacial energy due to impurities does not occur.

In conclusion, therefore, it would appear in the steels under this current investigation, that TME is a result of mainly interlath carbide formation upon decomposition of austenite due to tempering, i.e., the failure is primarily due to the microstructural influence on restricting slip to highly localized regions within laths. On the other hand, TE also occurs in some of these steels and appears to be an impurity-associated embrittlement (Figure 9), not so dependent on microstructure, but which can take over following TME if tempering is continued long enough for segregation to occur (e.g., the isothermal data of Figure 7).

Thus, the stability of retained austenite is of primary significance in controlling the properties of these medium carbon structural steels.

Considerable carbon partitioning has already been found in retained austenite where C levels of austenite rise above 2.5% and more than 5 at.% at the α'/γ interface.[33] So, in a strict sense, the transformation is not fully "martensitic".[37] Thus, in the TME condition, the interlath microstructure is very similar to that of upper bainite, but it is not yet certain whether the austenite actually decomposes by a bainitic mechanism. The instability of the austenite can be considered as follows.

The calculated TTT diagram is given in Figure 13 (broken lines) for one of the alloys containing 0.3 wt.% C. On the same graph, another TTT diagram (adapted from Ref. 38) is superimposed for an alloy corresponding to the composition found for the retained austenite (approximately 1 Wt.% C) in a 0.3% C steel. The critical tempering region (300-400°C), in which the steel containing retained austenite is tempered, corresponds to a temperature well above the Ms temperature of the carbon enriched retained austenite ($\sim$ 120°C), and is in the bainitic region for isothermal reactions. The microstructure now includes discontinuous stringers of carbides at the lath boundaries (Figure 14) due to austenite decomposition. This microstructure is similar to that found for upper bainite.[24]

CONCLUSIONS

1. The first minimum occurring in the mechanical properties (impact energy and tensile properties) is concurrent with the decomposition of retained austenite into M_3C carbides at the lath boundaries. The crystal structure of the carbide is orthorhombic. The carbides contain > 15% Cr when the alloys are tempered at 400°C for 135 hours. The decomposition of retained austenite is completed at 300°C for 1 hour in the Mn steels and at 400°C for 1 hour in Ni steel. However, by isothermal heat treatments

at lower temperatures for longer times, the decomposition reaction will occur.

2. TE occurs at 500°C for short tempering times (e.g., 1 hour) or can be induced at 400°C for longer tempering times (100 hours). It is associated with sulphur diffusion and segregation at the prior austenite grain boundaries. Therefore, the fracture is brittle and intergranular with respect to the prior austenite grain boundaries.

3. Since the C content of the as quenched retained austenite is about 1 wt.%, separate kinetics (i.e., TTT diagrams) must be considered for the retained austenite from that of the bulk alloy. The austenite films decompose to form discontinuous stringers of carbides at the lath boundaries. The overall result is the production of a microstructure that resembles upper bainite.

REFERENCES

1. G. Thomas: Met. Trans. A, 1978, vol. 9A, pp. 439-450.
2. C.J. McMahon and G. Thomas: Proceedings of the International Conference on the Microstructure and Design of Alloys, vol. 1, pp. 180-184, Inst. of Metals, London, 1973.
3. R.M. Horn and R.O. Ritchie: Met. Trans. A, 1978, vol. 9A, pp. 1039-1053.
4. B.V.N. Rao and G. Thomas: Met. Trans. A, 1980, Vol. 11A, pp. 441-457.
5. M. Sarikaya, B. Steinberg, and G. Thomas: University of California, Berkeley, California, unpublished research, 1982.
6. Annual Book of ASTM Standards, part 31, pp. 277-293 and 960-979, ASTM, Philadelphia, Pennsylvania, 1973.
7. L.J. Klinger, W.J. Barnett, R.P. Frohmberg, and A.R. Troiano: Trans. ASM, 1954, vol. 46, pp. 1557-1598.
8. B.R. Banerji: J. Iron and Steel Inst., 1965, vol. 203, pp. 166-174.

9. G.R. Speich and W.C. Leslie: Met. Trans., 1972, vol. 3, pp. 1043-1054.

10. G. Delisle and A. Galigois: J. Iron and Steel Inst., 1969, vol. 207, pp. 1628-1669.

11. Jr. Rellick and C.J. McMahon, Jr.: Met. Trans., 1974, vol. 5, pp. 2439-2450.

12. S.K. Banerji, C.J. McMahon, Jr., and H.C. Feng: Met. Trans. A, 1978, vol. 9A, pp. 237-247.

13. C.L. Briant, S.K. Banerji, and C.J. McMahon, Jr.: Fracture, vol. 1, pp. 363-385, Pergamon Press, New York, 1978.

14. J.E. King, R.F. Smith, and J.F. Knott: ibid, vol. 2,, pp. 279-286.

15. B.V.N. Rao and G. Thomas: J. of Fracture, 1977, vol. 13, pp. 705-709.

16. M.K.D.H. Bhadeshia and D.V. Edmonds: Metal Science, 1979, vol. 13, pp. 325-334.

17. C.L. Briant and S.K. Banerji: Met. Trans. A, 1981, vol. 12A, pp. 309-319.

18. B.C. Woodfine: J. Iron and Steel Inst., 1953, vol. 173, pp. 229-240.

19. J.M. Capus: J. Iron and Steel Inst., 1962, vol. 200, pp. 922-927.

20. J.R. Low, Jr., D.F. Stein, A.M. Turkalo, and R.P. Laforce, Trans. TMS-AIME, 1968, vol. 242, pp. 14-24.

21. H. Ohtani, H.C. Feng, and C.J. McMahon, Jr.: Met. Trans., 1974, vol 5, pp. 516-518.

22. J.E. King, R.F. Smith, and J.F. Knott: J. of Fracture, 1977, vol. 13, pp. 877-878.

23. G.Y. Lai, W.E. Wood, R.A. Clark, V.F. Zackay, and E.R. Parker: Met. Trans., 1974, vol. 5, pp. 1663-1670.

24. D.H. Huang and G. Thomas: Met. Trans., 1971, vol. 2, pp. 1587-1598.

25. M. Raghavan and G. Thomas: Met. Trans., 1971, vol. 2, pp. 3433-3439.

26. R.A. Clark and G. Thomas: Met. Trans. A, 1975, vol. 6A, pp. 969-979.

27. M.F. Carlson, B.V.N. Rao, and G. Thomas: Met. Trans. A, 1979, vol. 10A, pp. 1273-1284.

28. J.J. Hren, J.I. Goldstein, and D.C. Joy: Introduction to Analytical Electron Microscopy, pp. 121-167, Plenum Press, New York, 1979.

29. J. Chance and N. Ridley: Met. Trans. A, 1981, vol. 12A, pp. 1205-1213.

30. G. Thomas, M. Sarikaya, S.J. Barnard, and G.D.W. Smith: Proceedings of the Conference on Modern Developments in Physical Metallurgy of Steel, Inst. of Metals, London, in press.

31. R.L. Miller: Trans. ASM, 1964, vol. 57, p. 892.

32. S.J. Barnard, G.D.W. Smith, M. Sarikaya, and G. Thomas: Scripta Met., 1981, vol. 15, pp. 387-392.

33. M. Sarikaya, G. Thomas, J.W. Steeds, S.J. Barnard, and G.D.W. Smith: Proceedings of the International Conference on Phase Transformations, TMS-AIME, Pennsylvania, H.I. Aaronson and C.M. Wayman (eds.), in press.

34. H.W. Paxton and T. Kunitake: Trans. TMS-AIME, 1960, vol. 218, pp. 1003-1009.

35. M. Sarikaya and G. Thomas: Lawrence Berkeley Laboratory, University of California, Berkeley, and R.M. Fisher: U.S. Steel Corporation, Research Center, Monroeville, PA, unpublished research, 1981.

36. G. Thomas: Lawrence Berkeley Laboratory, University of California, Berkeley, CA, unpublished research, 1981.

37. G. Thomas and M.Sarikaya: Proceedings of the International Conference on Phase Transformations, TMS-AIME, Pennsylvania, H.I. Aaronson and C.M. Wayman (eds.), in press.

38. H. Tokushige: Lawrence Berkeley Laboratory, University of California, Berkeley, unpublished research, 1981.

39. Atlas of Isothermal Transformation and Cooling Transformation Diagrams, p. 218, American Society for Metals, Metals Park, OH, 1977.

Figure 1. A typical microstructure of the alloys (optical microscopy) showing packets of laths of martensite and prior austenite grain boundaries (alloy V1).

Figure 2. A composite of dark field electron micrographs showing the extent of retained austenite at the martensite lath boundaries.

Figure 3. Widmanstatten arrangement of Fe_3C within a martensitic lath is shown in (a) B.F. and (b) D.F. micrographs. Foil orientation is [111]. (Alloy V1 after 200°C tempering for 1 hour).

Figure 4. (a) B.F., (b) D.F., and (c) S.A.D. pattern from 2% Mn alloy after 300°C tempering for 1 hour. Carbides at the lath boundaries form from the decomposition of retained austenite which were identified to have Fe_3C structure from the S.A.D. pattern (c). Widmanstatten cementite which are also revealed in the D.F. micrograph also contribute to the S.A.D. pattern. The orientation relationship of the carbide is Bagaryatski.

Figure 5. Decomposition of retained austenite and the spheroidization of cementite at 400°C tempering (a) B.F. and (b) D.F. micrographs showing the carbide morphology at this tempering temperature for 1 hour. ($\frac{1}{2}$ - 2 Ni steel) (c) schematic illustration of the microstructure to distinguish between intralath and interlath carbides (trace of the D.F. micrograph) (d) carbide extraction replica micrograph of the alloy after 135 hours at 400°C showing extensive spheroidization, but morphologically similar to (a) and (b).

Figure 6. Charpy V-notch energy *vs.* tempering temperature curves reveal both TME and TE regions (1 hour tempering). Inset micrographs of V1 alloy show the corresponding dark field images: (a) retained austenite, (b) interlath carbides, (c) spheroidized intralath and interlath carbides in 2 Mn alloy. Values for the air melted alloys of the same compositions are also plotted for comparison (from Ref. 5).

Figure 7. Charpy V-Notch Energy vs. tempering curves for isothermal heat treatments. The drastic drop in the Charpy values of 2Mn alloy after 240°C tempering for 16 hours is due to TME (the fractograph is shown in Fig. 8d). Further decrease in fracture energy of this alloy occurs after long tempering at 400°C which is attributed to TE (refer to fractograph in Fig. 8f). On the other hand, prolonged heating in 1Mn alloys increases the impact values due to recovery and lower original retained austenite content.

Figure 8. Fracture surface analysis of the steels by SEM after different tempering conditions: a,b,g,i,j correspond to V1 (2 Mn alloy), h corresponds to V2 (2 Ni alloy) and c to f correspond to V3 (2 Mn alloy).

Figure 9. Typical Auger spectrum taken from the fractured surface of the 2 Mn alloy tempered at 400°C for 135 hours. Although S segregation was observed from temper embrittled specimens, no such segregations were revealed from the tempered martensite embrittled stage.

Figure 10. A typical atom probe spectrum showing the C concentration profile across martensite-austenite interface. (Specimen tempered at 200°C for 1 hour - 2 Mn alloy). Even in this condition, there is a considerable amount of C segregation at local regions along the interface. These regions are the probable nuclei for M_3C.

Figure 11. Change in the amount of retained austenite vs. time of tempering diagram for different isothermal treatments. X is the volume % of retained austenite in the bulk material determined by X-ray analysis.

Figure 12a. Scheme showing the observations of in-situ fracture of foils, suggesting the influence of microstructure on plastic zone and fracture path. The carbon contents in γ correspond to the FIM atom probe data (Ref. 32).

Figure 12b. Slip within a martensite lath could lead to immobile [01T] type dislocations. Slip also occurs on the {110} planes containing intralath Fe_3C after tempering, giving rise to local zig-zag fracture.

Figure 13. Superimposed TTT diagrams reproduced for the bulk alloy containing 0.3 wt.% C (Ref. 38) and to the imaginary alloy of the C composition corresponding to that of retained austenite, i.e., 1 wt.% (Ref. 39). Tempering the bulk alloy at 300°C will cause the retained austenite to decompose in the upper bainitic region.

Figure 14. High magnification (a) B.F. and (b) D.F. micrographs reveal the "islands" of M_3C particles formed as a result of the decomposition in a 2 Mn alloy after 400°C tempering (1 hour).

ACKNOWLEDGEMENTS

This work was supported by the Director, Office of Energy Research, Office of Basic Energy Sciences, Division of Materials Sciences of the U.S. Department of Energy under Contract No. DE-AC03-76SF00098.

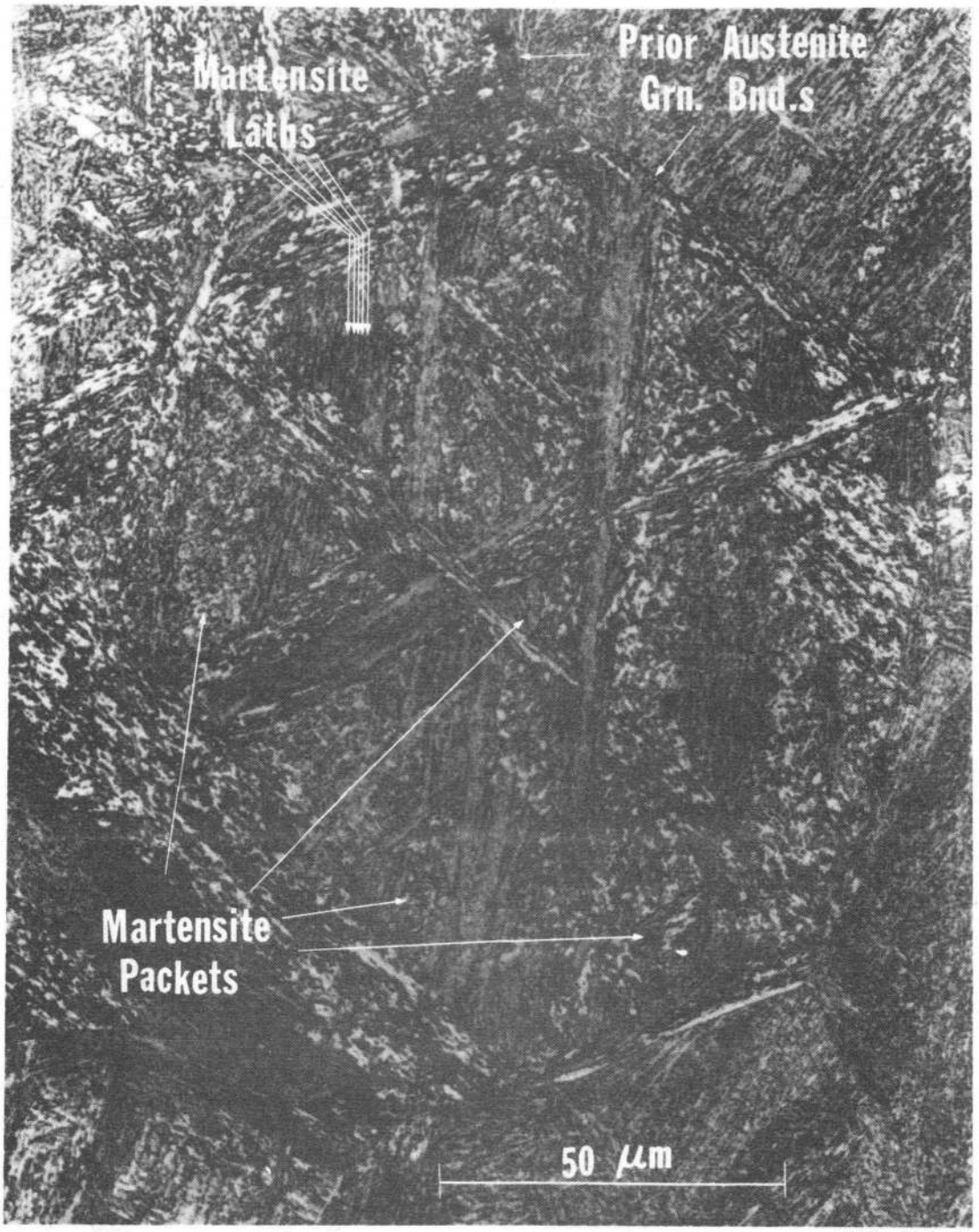

XBB 821-5

Fig. 1

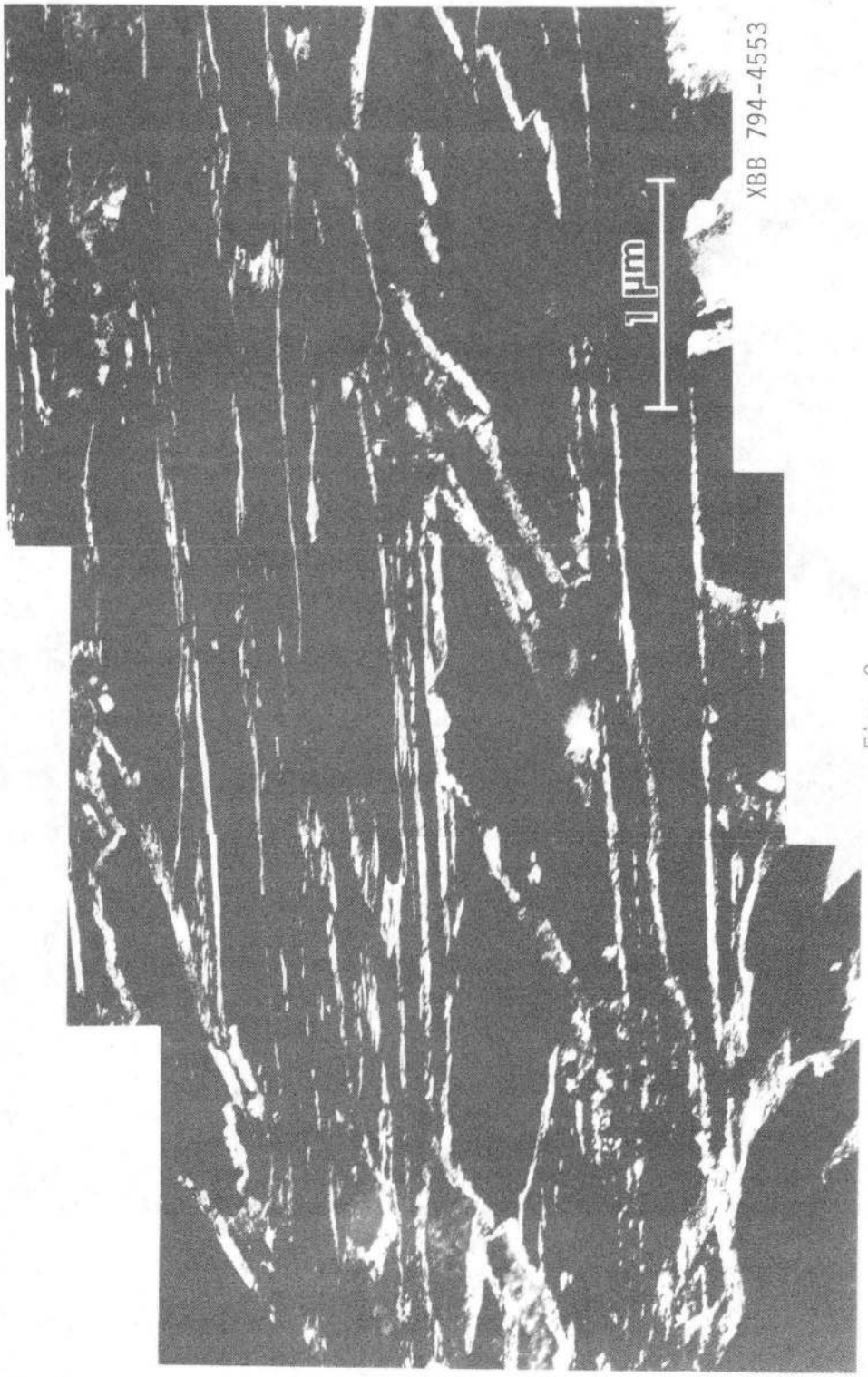

Fig. 2

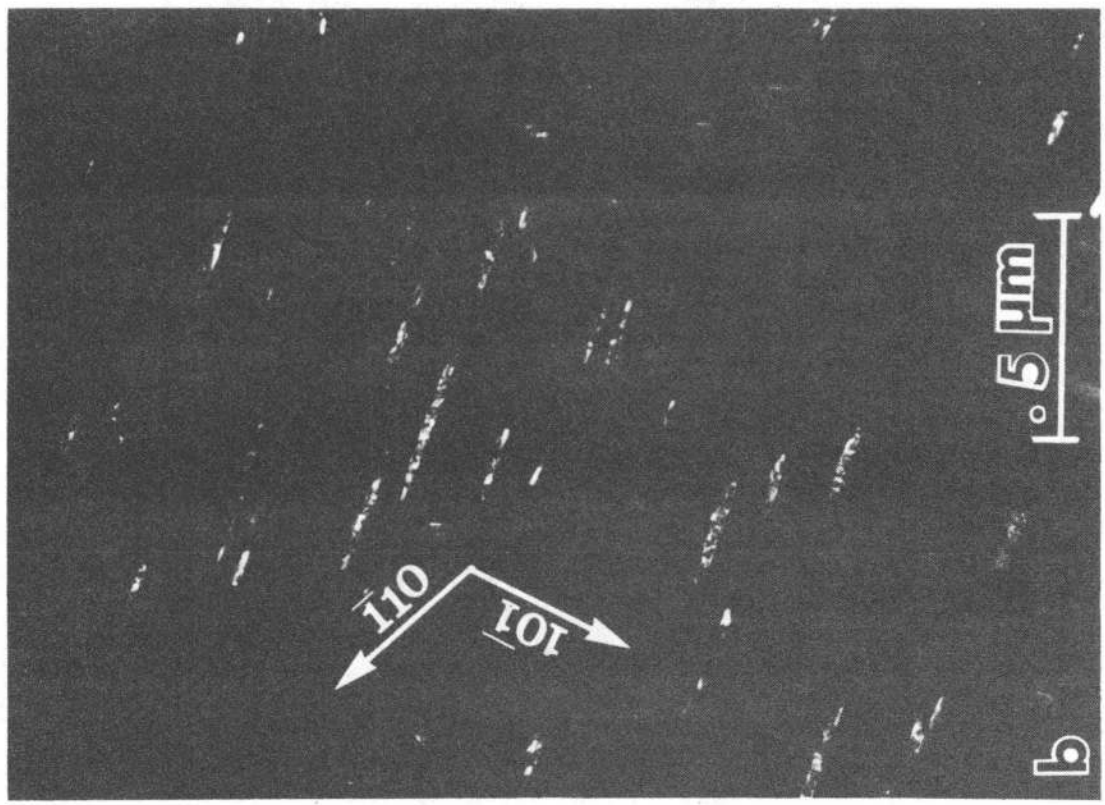

Fig. 3

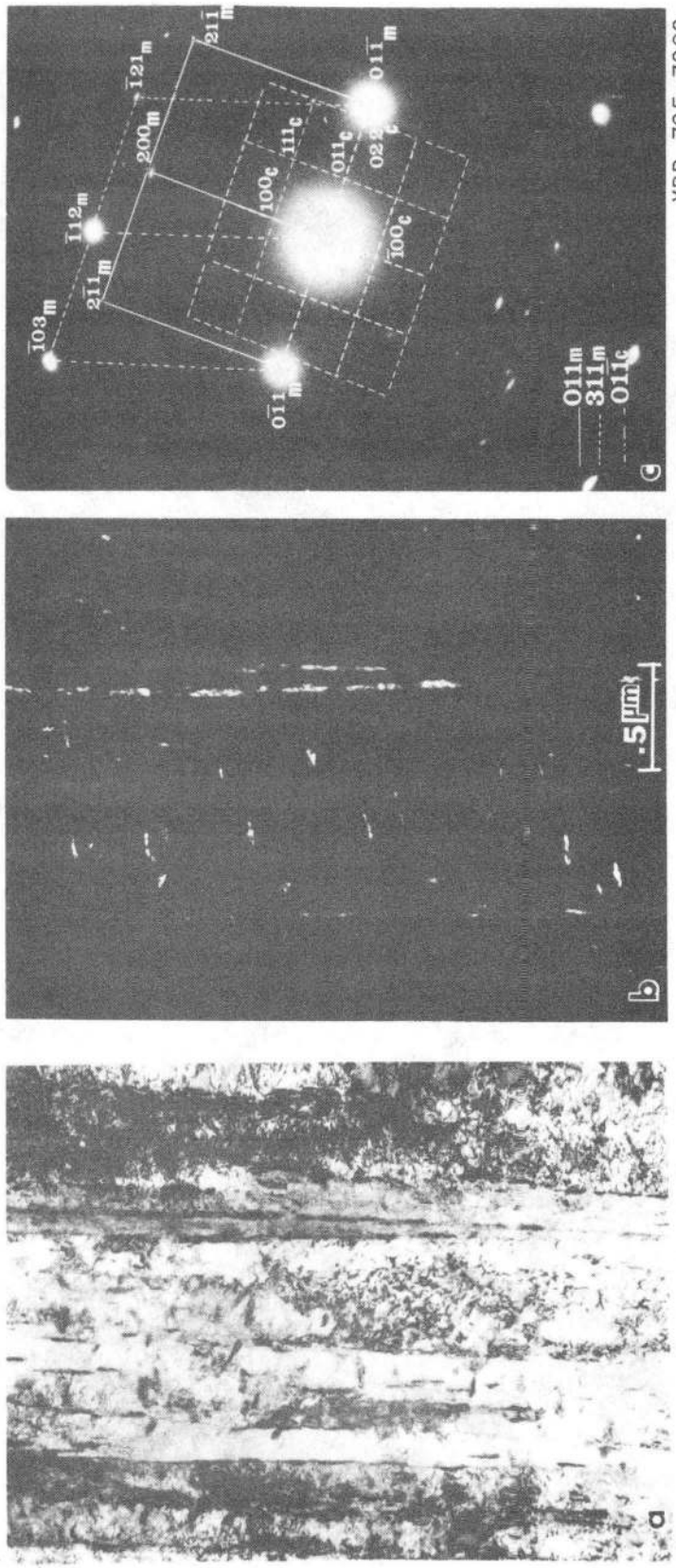
a
b
.5 μm
c
$\bar{1}03_m$
$\bar{1}12_m$
$2\bar{1}1_m$
200_m
$\bar{1}21_m$
$2\bar{1}\bar{1}_m$
$0\bar{1}1_m$
100_c
$\bar{1}11_c$
011_c
$02\bar{2}_c$
$0\bar{1}\bar{1}_m$
$\bar{1}00_c$
011_m
311_m
$01\bar{1}_c$
XBB 795-7089

Fig. 4

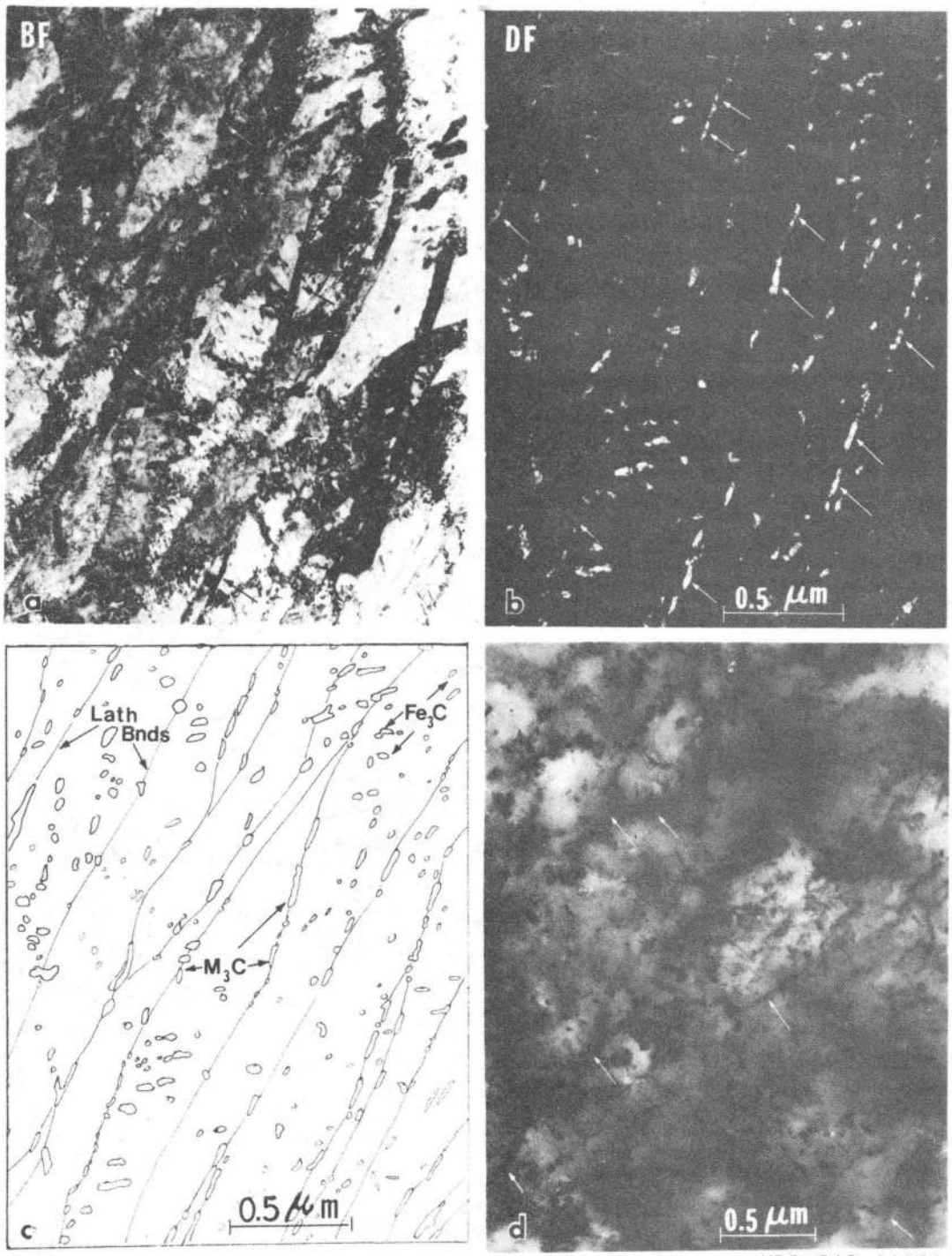

XBB 810-11861

Fig. 5

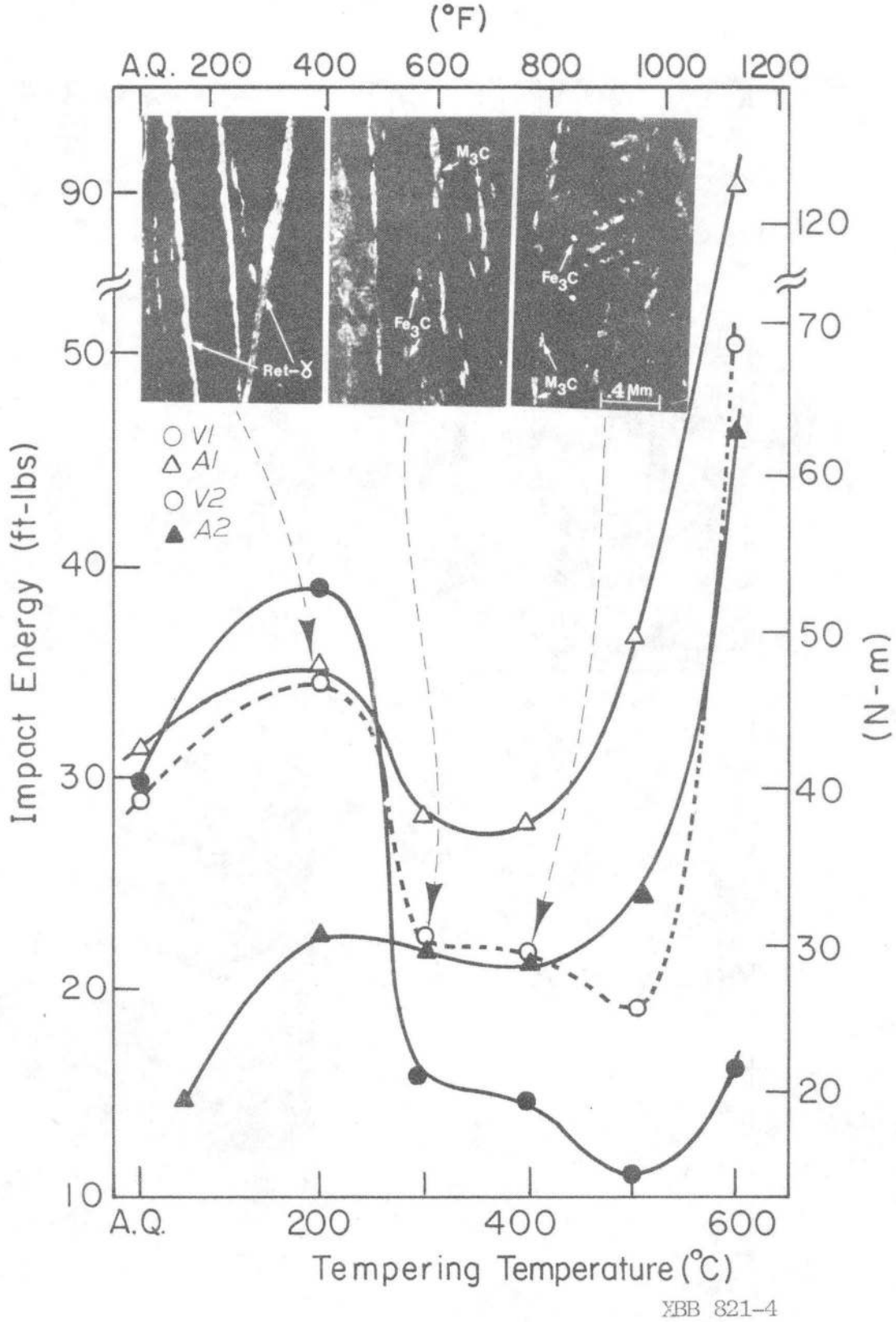
(°F)
A.Q. 200 400 600 800 1000 1200
Ret-γ
M3C
Fe3C
Fe3C
M3C
.4 Mm
V1
A1
V2
A2
Impact Energy (ft-lbs)
(N-m)
90
50
40
30
20
10
120
70
60
50
40
30
20
A.Q. 200 400 600
Tempering Temperature (°C)
XBB 821-4

Fig. 6

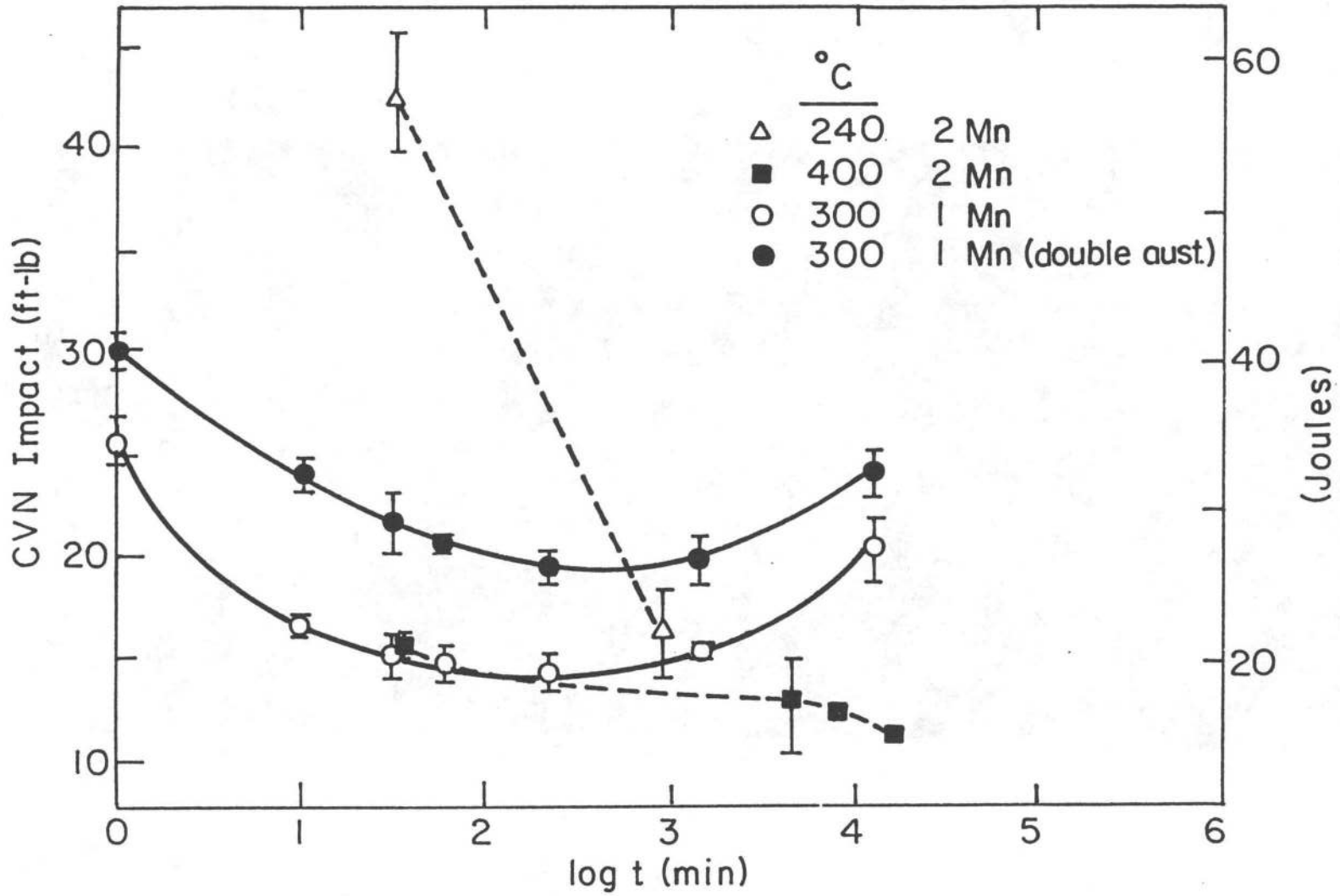
°C
240 2 Mn
400 2 Mn
300 1 Mn
300 1 Mn (double aust.)
CVN Impact (ft-lb)
(Joules)
log t (min)
10
20
30
40
60
0
1
2
3
4
5
6
XBL 824-5548

Fig. 7

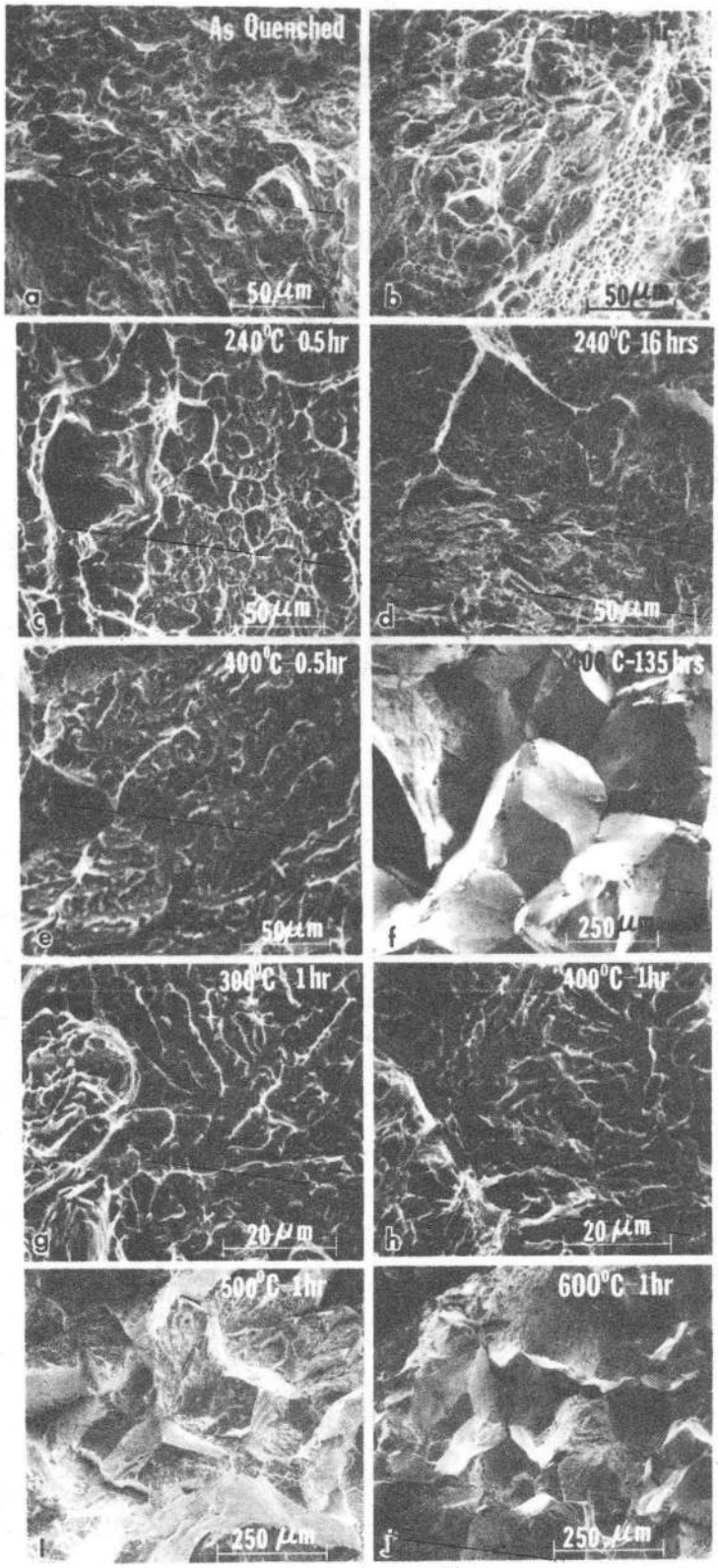

XBB 821-3

Fig. 8

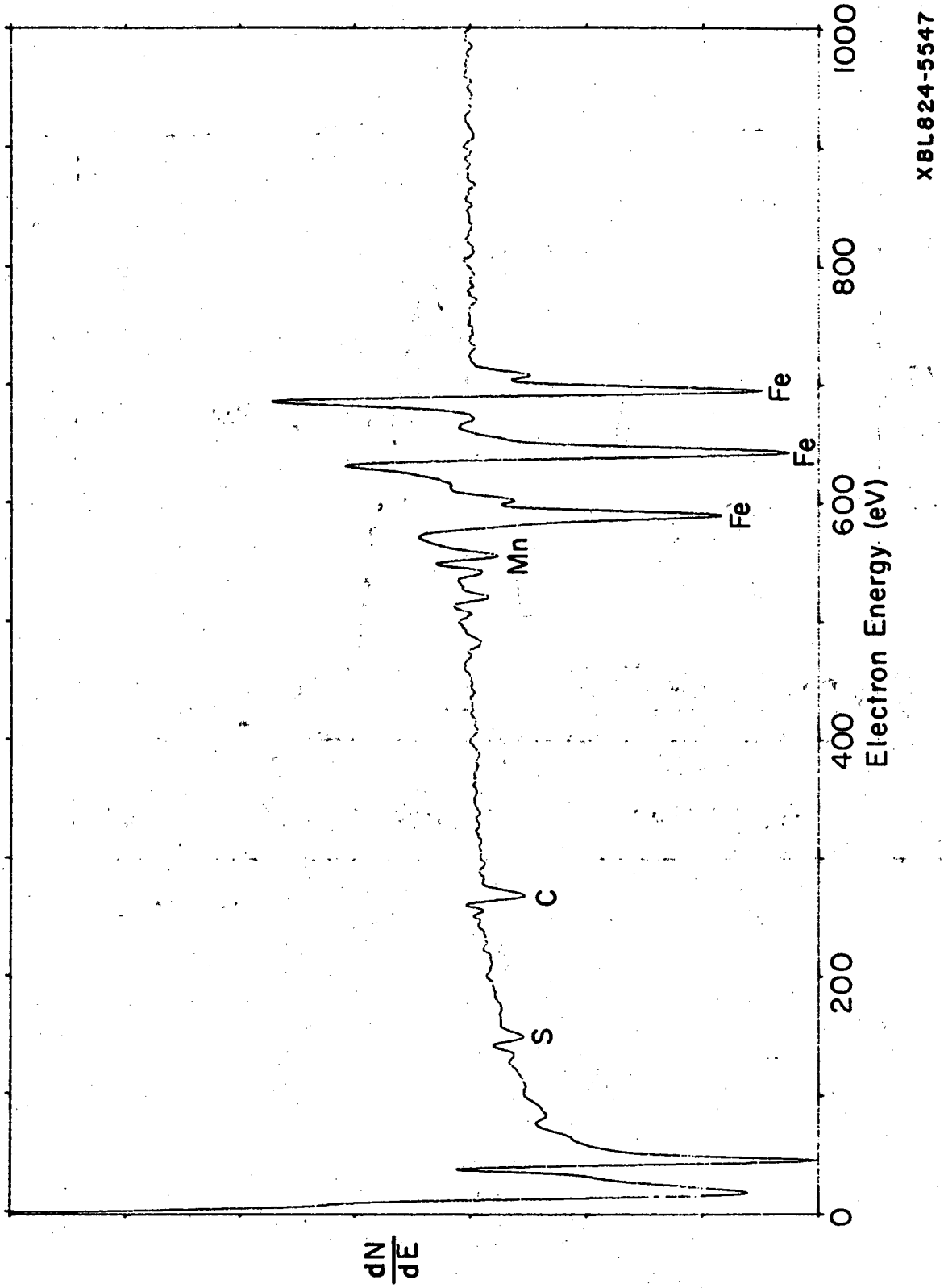
dN/dE
0
200
400
600
800
1000
Electron Energy (eV)
S
C
Mn
Fe
Fe
Fe
XBL824-5547

Fig. 9

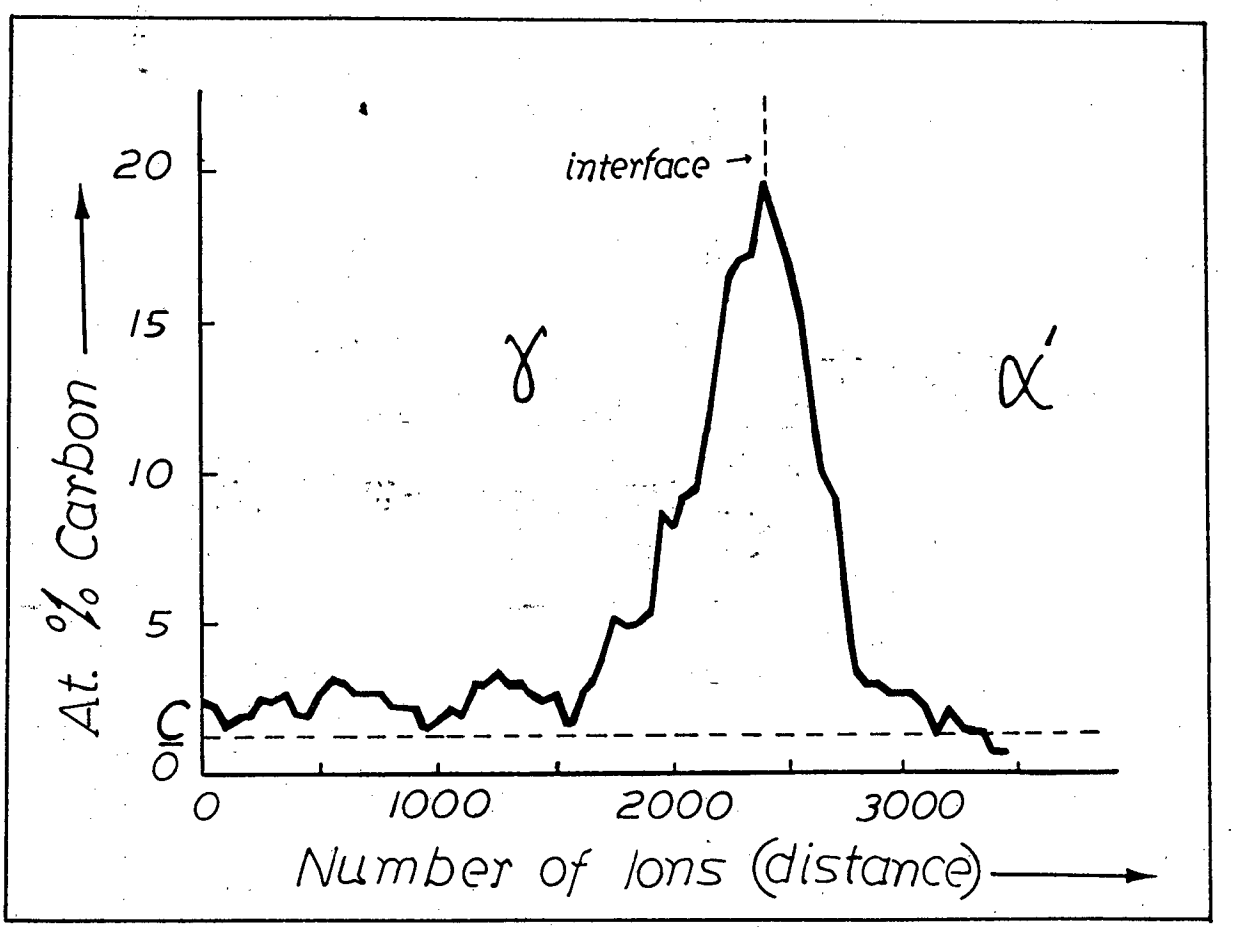

XBL 824-9292

Fig.10

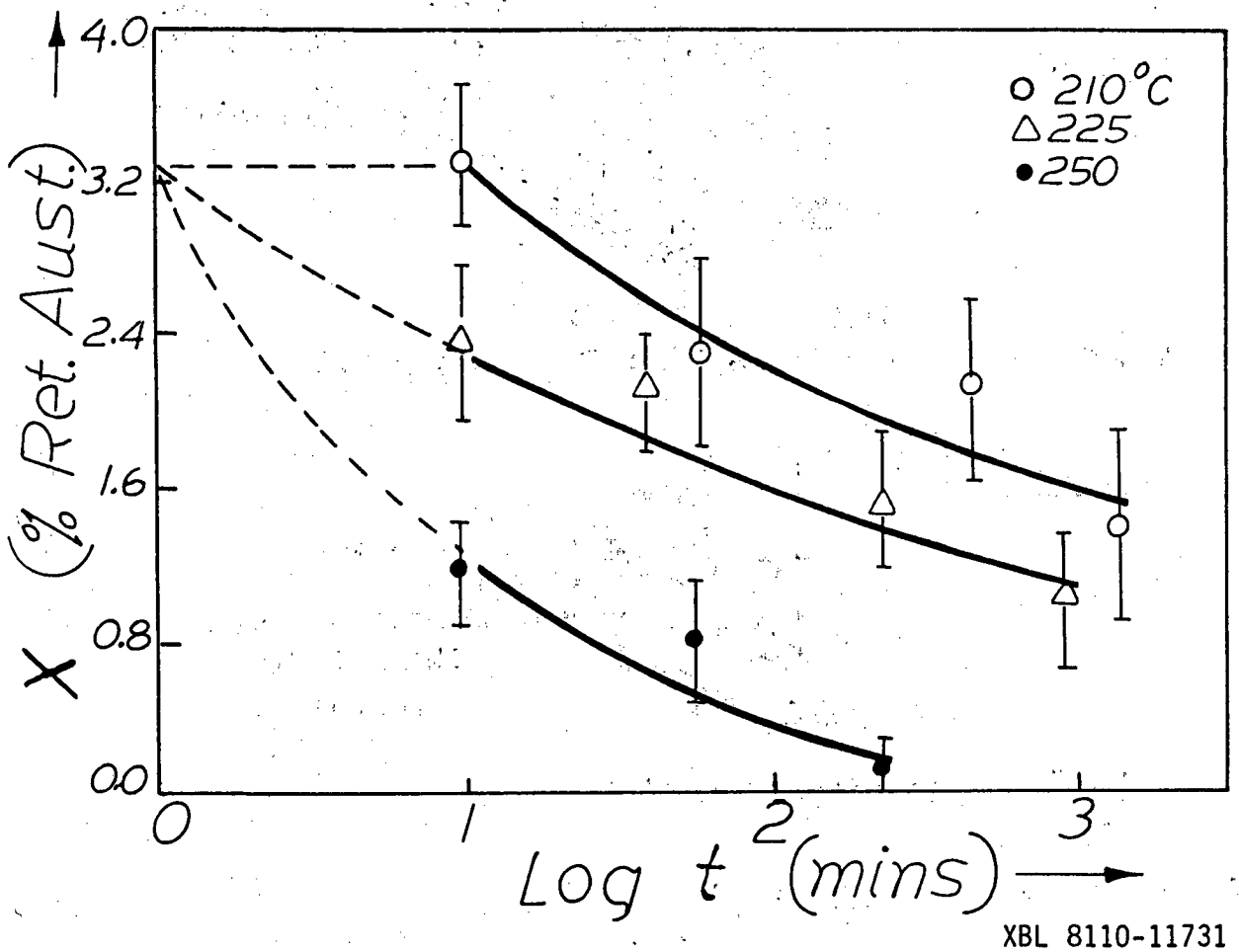
4.0
3.2
2.4
1.6
0.8
0.0
X (% Ret. Aust.)
0
1
2
3
Log t (mins)
○ 210°C
△ 225
● 250
XBL 8110-11731

Fig. 11

FRACTURE IN DISLOCATED MARTENSITE

ORIENTATION 1-2-3 SIMILAR

1. AS QUENCHED

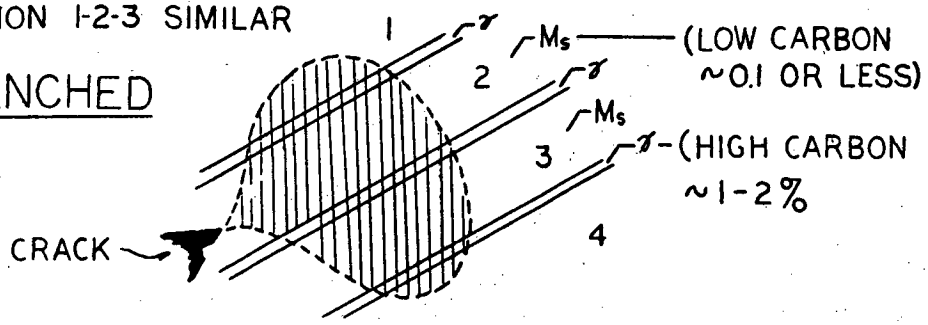

DUCTILE VOID COALESCE

MICRO SLIP CONTIGUOUS ACROSS γ/M_s, $f \sim 10^{12}$

2. TEMPERED (TME)

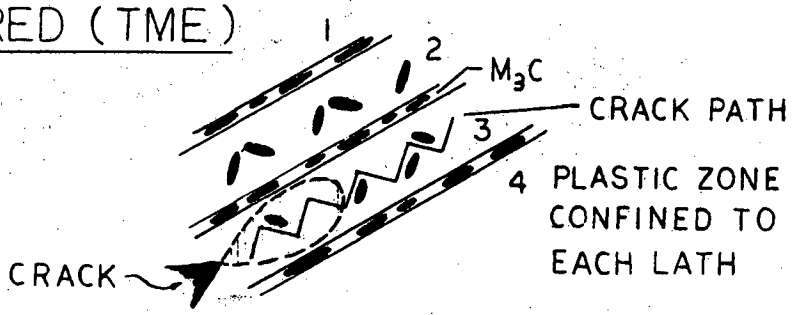

MICRO CLEAVAGE-LIKE, BRITTLE

3. TEMPERED (COARSED)

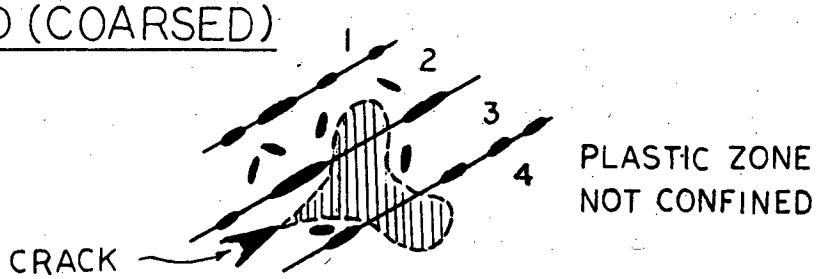

MICRO SLIP DUCTILE

SLIP ON {111} PLANES WITHIN MARTENSITE IS ALSO RESTRICTED DUE TO {110} CARBIDES

PLASTIC ZONE DEFECT BY MICRSTRUCTURE (CARBIDE MORPHOLOGY)

XBL 824-9220

Fig.12a

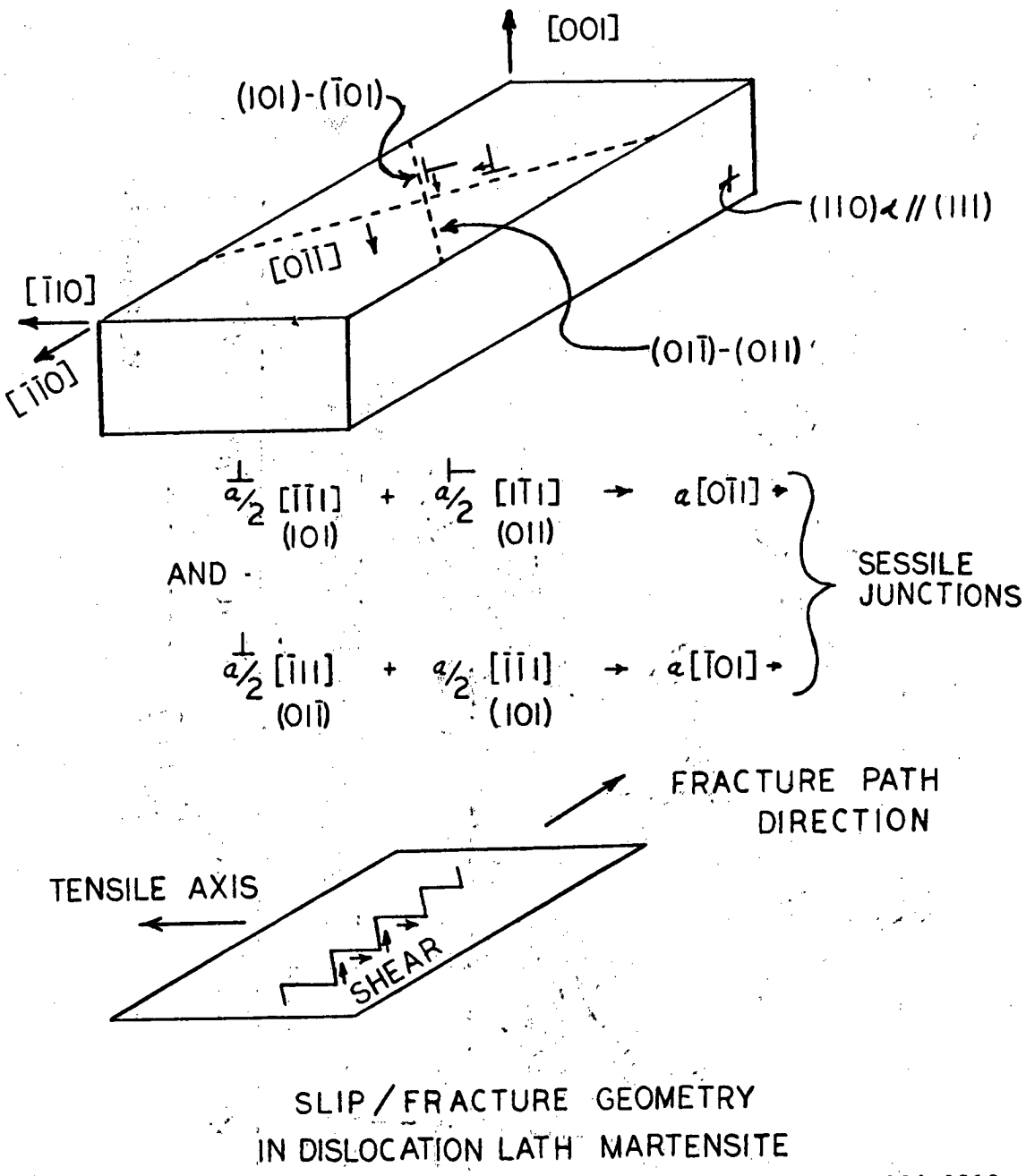

SLIP / FRACTURE GEOMETRY
IN DISLOCATION LATH MARTENSITE

XBL 824-9219

Fig. 12b

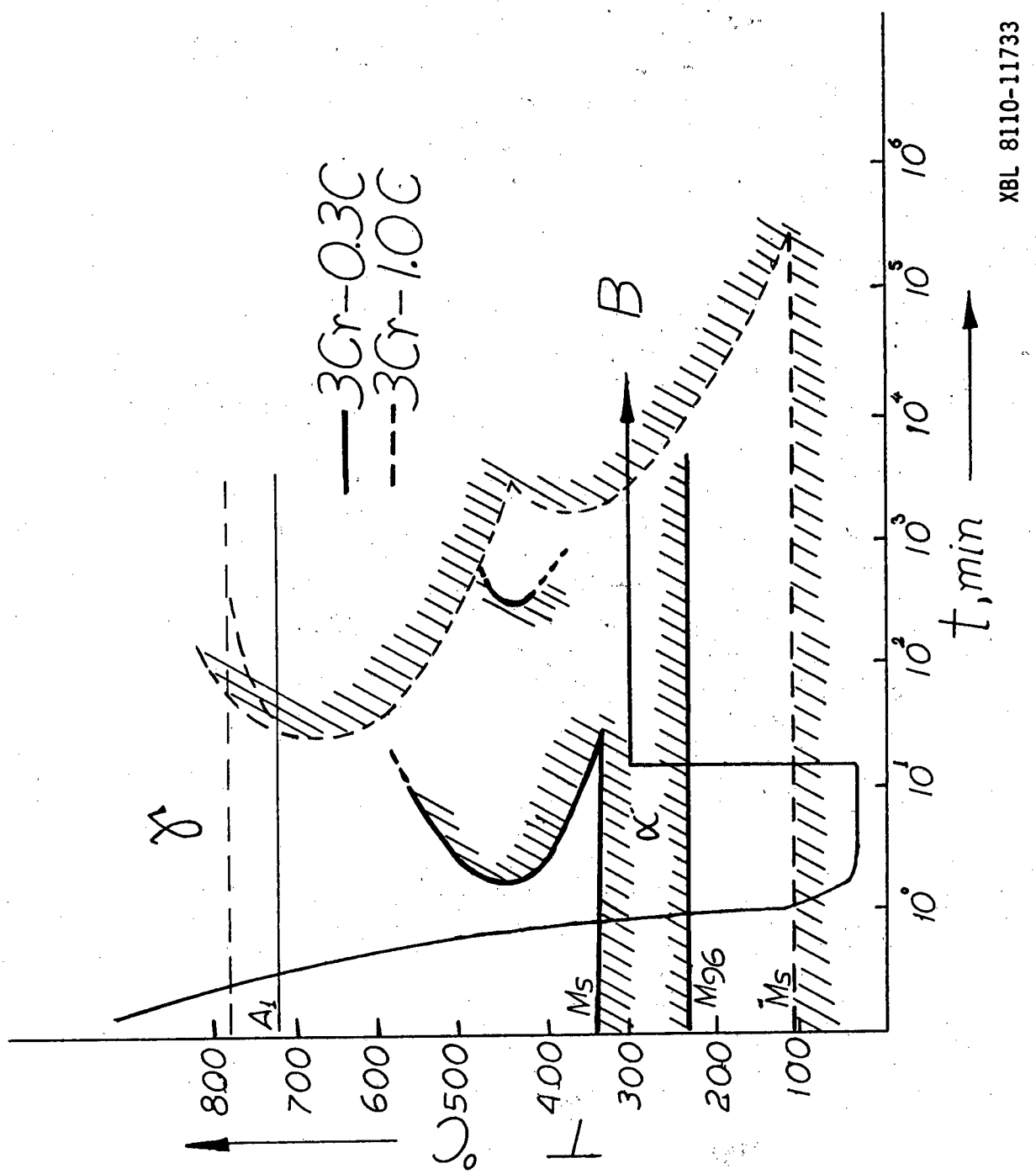

XBL 8110-11733

Fig. 13

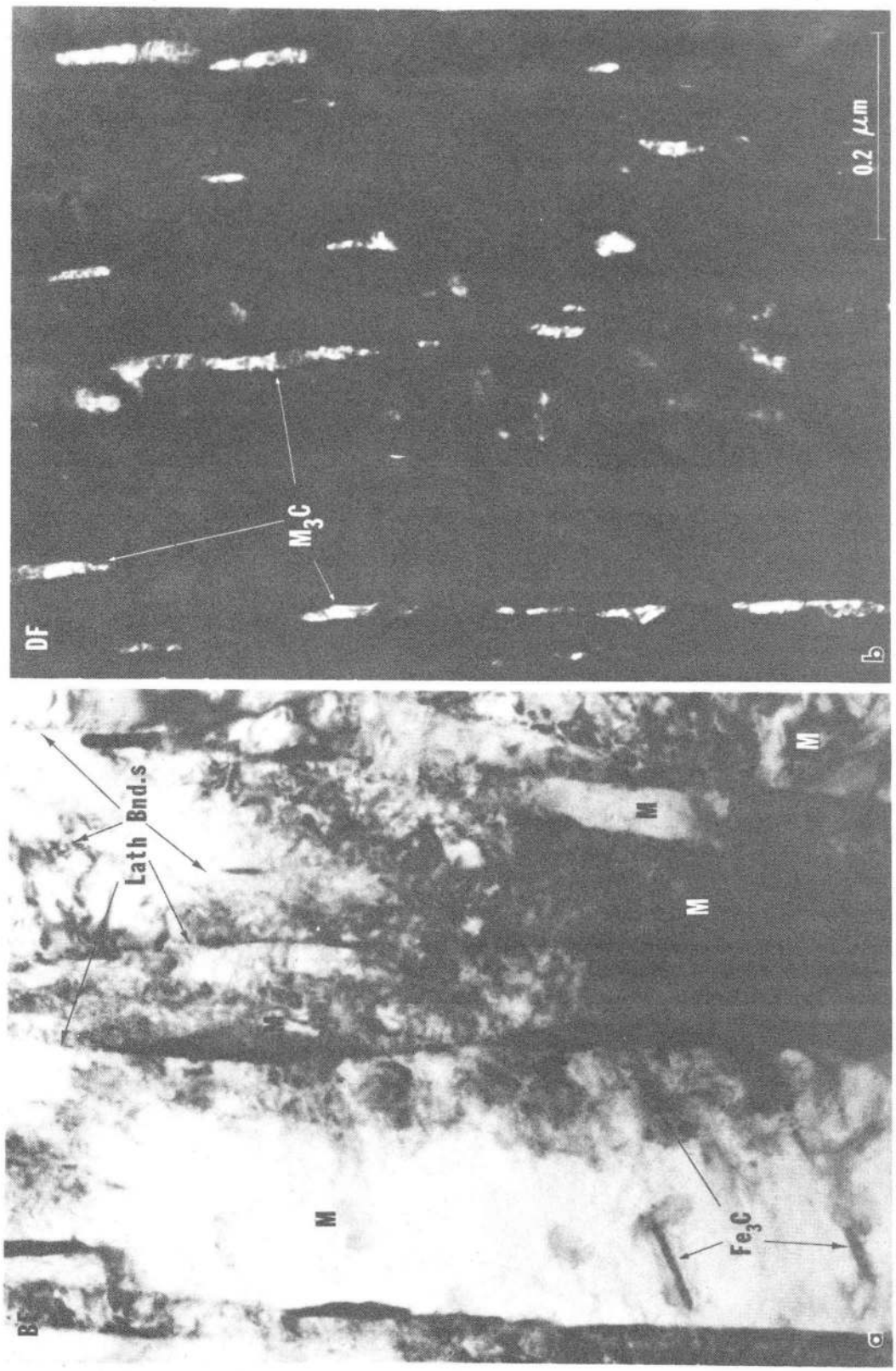

XBB 821-2

Fig. 14

TECHNICAL INFORMATION DEPARTMENT
LAWRENCE BERKELEY LABORATORY
UNIVERSITY OF CALIFORNIA
BERKELEY, CALIFORNIA 94720